

## BVRI PHOTOMETRIC CALIBRATION OF THE NEDELJKOVIĆ TELESCOPE

A. Vudragović and M. I. Jurkovic

*Astronomical Observatory, Volgina 7, 11060 Belgrade, Serbia*

E-mail: [ana@aob.rs](mailto:ana@aob.rs)

(Received: April 4, 2021; Accepted: July 5, 2021)

**SUMMARY:** We have done photometric calibration of the 60 cm Nedeljković telescope equipped with the FLI PL 230 CCD camera, mounted at the Astronomical Station Vidojevica (Serbia), using standard stars from the Landolt catalog. We have imaged 31 fields of standard stars using Johnson's *BVRI* filters during three nights in August 2019. We have measured both extinction and color correction. Relating our calibrated magnitudes to the magnitudes of standard stars from the Landolt catalog, we have achieved accuracy of 2%-5% for the *BVRI* magnitudes.

**Key words.** Techniques: photometric – Stars: imaging

### 1. INTRODUCTION

The Astronomical Station Vidojevica<sup>1</sup> (ASV) hosts several telescopes used for various observing projects led by the Astronomical Observatory in Belgrade. It is located on the Vidojevica mountain top in the south of Serbia. For more information on the ongoing observing projects see [Vince et al. \(2014\)](#). The ASV has the following telescopes:

- o Milanković (1.4 m) telescope,
- o Nedeljković (60 cm) telescope, and
- o MEADE 40 cm telescope.

The 60 cm Nedeljković telescope (Cassegrain type) has been in use since 2011 ([Vince and Jurkovic 2012](#)). In this article we describe the photometric calibration carried out on this telescope during 2019 introducing a new observational project: the observation of pulsating stars. The CCD camera on the telescope is FLI PL 230.

In order to calibrate magnitudes and colors of any object, one needs to observe many standard stars fields, well distributed on the sky at different time during the night, making sure their colors cover the range of the target's color. These standard stars are used to define our photometric system through a set of calibration equations that relate instrumental and calibrated magnitudes. Solving a set of calibration equations determines calibration coefficients, that transform instrumental magnitudes into the calibrated magnitudes. A detailed description of the photometric procedures applicable in astronomical measurements is given in ([Henden and Kaitchuck 1982](#)).

In this paper we describe a selection of standard stars used to perform photometric calibration in Section 2. In Section 3 we provide description of the data reduction procedure used. Photometric calibration is introduced in Section 4 where two different models (approaches) are discussed. Finally, in Section 5 we test these different models and provide relevant coefficients for photometric transformation to the standard Landolt photometric system for the *BVRI* filters, and briefly discuss photometric conditions in Section 6.

---

© 2021 The Author(s). Published by Astronomical Observatory of Belgrade and Faculty of Mathematics, University of Belgrade. This open access article is distributed under CC BY-NC-ND 4.0 International licence.

<sup>1</sup><http://vidojevica.aob.rs>

**Table 1:** The observational log of the Landolt fields: field name is given in the first column, followed by its right ascension and declination. Fields are listed in the order of time of observations, divided into three nights.

Field	RA[h:m:s]	DEC[d:m:s]
5th August, 2019		
GD2	00:07:33.56	+33:18:51.2
PG1648+536	16:49:59.88	+53:29:15.7
GD 363	17:38:37.20	+41:53:20.4
GD 378	18:23:40.51	+41:05:23.2
GD 391	20:29:50.05	+39:15:53.2
KUV 433-03	16:38:27.06	+34:59:59.2
PG1430+427	14:32:33.67	+42:31:19.1
SA 35 SF1	15:49:51.49	+44:31:38.6
SA 38 SF1	18:47:35.13	+45:10:43.7
SA 38 SF4	18:50:37.38	+45:08:17.9
SA 41 SF1	21:53:39.41	+45:35:12.1
SA 41 SF2	21:54:18.29	+45:14:52.4
GD 336	14:31:54.90	+37:06:03.3
6th August, 2019		
GD 13	01:29:41.71	+42:28:06.5
GD 275	01:18:54.23	+52:27:31.8
GD 277	01:29:26.95	+51:08:41.0
GD 278	01:31:02.37	+53:21:17.5
GD 279	01:52:02.42	+47:01:04.7
GD 405	23:16:44.42	+47:27:07.7
GD 421	01:51:00.14	+67:41:51.4
SA 23 SF1	03:44:25.66	+45:06:55.1
SA 23 SF2	03:44:43.72	+45:20:43.1
7th August, 2019		
GD 10	01:06:59.69	+39:31:14.1
GD 325	13:36:16.80	+48:29:31.9
GD 8	00:39:44.65	+31:34:46.3
PG1343+578	13:45:03.08	+57:31:12.1
SA 20 SF1	00:44:47.51	+45:50:05.3
SA 20 SF2	00:45:24.64	+45:41:44.2
SA 20 SF3	00:45:36.80	+45:52:21.4
SA 20 SF4	00:46:34.53	+46:06:53.6
SA 20 SF5	00:46:56.20	+45:52:49.4

## 2. OBSERVATIONS

The observations were done on the 5th, 6th and 7th August, 2019. The individually observed photometric standards were taken from the (Landolt 2013). The Landolt catalog contains 258 standard stars in 156 fields each having a  $6'.8 \times 6'.8$  field of view. The field of view of our instrumentation was  $17'.7 \times 17'.8$ . Selected Landolt fields with their celestial coordinates are listed in Table 1, grouped by the date observed.

Each night, calibration frames were taken along with science frames: flat, bias and dark frames. The color range of standard stars is chosen to be  $B - V = (0.0, 1.3)$ . In total, we have observed 31 Landolt fields. Due to the limitations imposed by telescopes's motors, the fields that were close to the zenith could not be observed. This resulted in observations of Landolt fields only for up to the  $60^\circ$  height above the horizon.

## 3. DATA REDUCTION

All raw images were first astrometrically solved and reduced. The astrometric solution was obtained using Astrometry software (Lang et al. 2010). Seven frames in the  $B$ -band were not successfully solved initially due to either insufficient flux or tracking errors. These frames were smoothed with Gaussian filter and then astrometrically solved. Data reduction was done following the standard procedure based on the Milankovic pipeline (Müller et al. 2019). The master bias frame was constructed for each night as a median of all bias frames and subtracted from each science frame. The master dark frame was created from individual dark frames of the largest exposure time for the particular night scaled to correspond to individual exposures. The master bias frame was subtracted from each flat field image, along with the master dark frame of the same exposure time (a 5 second exposure). Afterwards, each flat field image was normalized to its median value in each of the filters ( $B$ ,  $V$ ,  $R$  and  $I$ ) and the median stack was created as the final master flat. Then, the science frames were divided by these master flat frames. These fully reduced science frames were then fed into the Python script that measured the magnitudes of the stars selected based on their celestial coordinates. Aperture photometry was done inside apertures 3.3 times larger than the FWHM =  $4.5 \text{ pix} = 2.7 \text{ arcsec}$  using the `Photutils` package<sup>2</sup> (Bradley et al. 2020). In the sky annulus (10 pixels wide) around each star mask was created by sigma clipping to exclude any other object if present. Instrumental magnitudes were measured according to the standard formula:

$$m = -2.5 * \log F + 2.5 \log t, \quad (1)$$

$$F = \sum C_i - As, \quad (2)$$

where  $C_i$  are counts measured in the aperture,  $F$  is the flux,  $A$  is the aperture area,  $s$  is the sky measured inside the sky annulus divided by its area (sky per pixel), and  $t$  is the observational time in seconds.

Errors in magnitudes ( $\Delta m$ ) were calculated using formula from IRAF's `phot` package slightly modified:

<sup>2</sup>`Photutils` is an open source Python package (a part of the Astropy project) that provides tools including, but not limited to the aperture photometry (<https://photutils.readthedocs.io/en/stable/>)

$$\Delta m = 1.0857 \Delta F / F,$$

$$\Delta F = \sqrt{F + A\sigma^2 + A^2\sigma^2/S},$$

where  $\sigma$  is the standard deviation of the background inside the sky annulus and  $S$  is the area of the sky annulus.

In Table 2, all observed and processed fields are listed. For each of the *BVRI* filters the number of stars is indicated in the column labeled with  $N$ . The PG1343+578 field was excluded from further analysis, since only the *B*- and *V*-frames were imaged thus lacking the color information that is needed for photometric calibration. In total, there are 154 stars in 30 Landolt fields for the subsequent photometric calibration.

#### 4. PHOTOMETRIC CALIBRATION

The aim of this work is to relate instrumental magnitudes measured at the ASV with the 60 cm Nedeljković telescope equipped with the FLI PL 230 CCD camera to magnitudes of the standard stars selected from the catalog of Landolt (2013). The calibrated magnitudes we wish to determine are those measured with the detector that perfectly matches the standard *BVRI* system operating above the atmosphere. Both magnitudes and colors should match the chosen standard system measurements. The photometric calibration consists of correcting two effects: (1) the atmospheric extinction and (2) mismatch between the instrumental and standard system.

First, instrumental magnitudes need to be corrected for atmospheric extinction or dimming of the starlight by the earth's atmosphere. The longer the path of the light the more it is dimmed<sup>3</sup>. The length of this path is called the air mass. We can relate the magnitude of the object above the atmosphere  $m_0(\lambda)$  for any particular wavelength  $\lambda$  to  $m_i$ , measured at the surface of the earth:

$$m_0(\lambda) = m_i(\lambda) + k(\lambda)X(z), \quad (3)$$

where  $X(z)$  is the air mass and  $k(\lambda)$  is the extinction coefficient at the zenith distance  $z$ . The air mass  $X$  can be approximated for small zenith angles with  $X = \sec z$ , where  $z$  is the zenith distance. A more precise relationship is given in Young and Irvine (1967). The air mass is calculated automatically and added to the header of images during the observing session. The air mass range spans from 1 to 1.5. The extinction coefficient can be determined as the slope of the relation between the instrumental magnitude and the air mass. During the night, the target stars will be at different air masses and, from the simple

<sup>3</sup>A star closer to the horizon will dim more than the one closer to the zenith.

linear relation Eq. (3), we can determine the extinction coefficient for a specific filter used. The extinction coefficient is dependent on the wavelength since shorter wavelengths (blue light) scatter more than longer ones (red light); one need to measure extinction coefficient for each filter separately.

The second effect, a possible mismatch between our instrumentation and Landolt's, can be corrected by adding another term to Eq. 3, the so-called color term ( $\epsilon$ ):

$$m_{\text{std}}(\lambda) = m_0(\lambda) + \epsilon C, \quad (4)$$

where  $C$  is the color, and  $m_{\text{std}}$  the standard magnitude. This correction can only be done if more than one filter is being used, since color is the difference between magnitudes in the two bands. For every combination of magnitudes and colors, one such equation can be written, thus a system of linear equations need to be solved to standardize the instrumental system used.

Another problem is related the the blue band, since, as we have already pointed out, shorter wavelengths scatter more than longer ones and thus we might expect a dependence of the extinction coefficient on color. In the blue band, another term can appear (complicating the equation Eq. 3), the co-called secondary extinction coefficient ( $k''$ ):

$$k(\lambda) = k'(\lambda) + k''(\lambda) C. \quad (5)$$

##### 4.1. Calibration without color correction

We will consider here the case when the instrumental system is perfectly matched to the standard one. In this case, the only correction that need to be applied is the extinction correction. This correction will give us magnitudes that are measured above the atmosphere with the combination of filters and a detector that match the one used in the standard *BVRI* system.

Equations that relate instrumental magnitudes measured (Eq. 1) on the terrestrial surface to those that would be measured above the atmosphere, thus correcting for the dimming of starlight caused by light passage trough the atmosphere, are:

$$b_0 = b_i - k_b X, \quad (6)$$

$$v_0 = v_i - k_v X, \quad (7)$$

$$r_0 = r_i - k_r X, \quad (8)$$

$$i_0 = i_i - k_i X, \quad (9)$$

where *BVRI* denotes the measured magnitudes (suffix 0 correspond to the ones measured above atmosphere and suffix *i* to instrumental magnitudes) and  $k_{b,v,r,i}$  is the extinction coefficient in the corresponding band.

Matching them with the standard system reduces the calibration equations to a set of simple linear equations with only a constant offset (magnitude

**Table 2:** List of standard stars' fields selected for photometric calibration and observed at the ASV with the 60 cm Nedeljković telescope equipped with a FLI PL 230 CCD camera. The first column is the Landolt field; the second column lists the number of stars in that field; starting from the third column each group of three columns gives: a specific filter (f) indicated by the letter *B*, *V*, *R* or *I*, the air mass (*X*) and the exposure time of individual science frames in seconds (Exp) corresponding to the indicated filter. Since there are 4 different filters, there are 12 columns in total for each of the fields selected from the Landolt catalog of standard stars labeled in the first column.

Field	<i>N</i>	f	<i>X</i>	Exp									
GD 2	6	B	1.01	180	V	1.01	100	R	1.01	100	I	1.01	100
GD 8	4	B	1.08	600	V	1.09	300	R	1.07	300	I	1.06	300
GD 10	4	B	1.02	300	V	1.02	200	R	1.01	230	I	1.01	250
GD 13	2	B	1.31	300	V	1.32	120	R	1.29	120	I	1.28	120
GD 275	2	B	1.45	300	V	1.56	200	R	1.43	200	I	1.40	200
GD 277	3	B	1.39	300	V	1.35	180	R	1.34	180	I	1.33	180
GD 278	3	B	1.20	300	V	1.21	180	R	1.19	180	I	1.18	180
GD 279	10	B	1.11	90	V	1.11	45	R	1.10	45	I	1.10	45
GD 325	4	B	2.18	300	V	1.72	150	R	1.78	150	I	2.15	150
GD 336	4	B	1.52	120	V	1.54	60	R	1.55	60	I	1.57	60
GD 363	5	B	1.19	180	V	1.21	90	R	1.22	120	I	1.22	120
GD 378	4	B	1.20	130	V	1.22	80	R	1.23	80	I	1.23	80
GD 391	9	B	1.06	230	V	1.07	100	R	1.07	100	I	1.07	100
GD 405	2	B	1.43	300	V	1.40	150	R	1.31	120	I	1.30	120
GD 421	5	B	1.18	180	V	1.20	120	R	1.19	90	I	1.19	90
KUV 433	2	B	1.26	150	V	1.27	90	R	1.28	100	I	1.29	100
PG1430+427	4	B	1.51	120	V	1.54	80	R	1.58	30	I	1.59	30
PG1648+536	6	B	1.21	90	V	1.22	25	R	1.23	10	I	1.23	10
PG1343+578	2	B	1.92	500	V	1.89	200	/	/	/	/	/	/
SA 20 SF1	4	B	1.02	30	V	1.02	15	R	1.02	15	I	1.02	15
SA 20 SF2	5	B	1.02	30	V	1.02	15	R	1.02	15	I	1.02	15
SA 20 SF3	4	B	1.02	30	V	1.02	15	R	1.02	15	I	1.02	15
SA 20 SF4	5	B	1.02	50	V	1.01	25	R	1.01	25	I	1.01	25
SA 20 SF5	9	B	1.01	60	V	1.01	30	R	1.01	30	I	1.01	30
SA 23 SF1	5	B	1.32	45	V	1.31	20	R	1.31	10	I	1.30	5
SA 23 SF2	5	B	1.30	45	V	1.29	20	R	1.29	20	I	1.28	10
SA 35 SF1	4	B	1.29	10	V	1.29	5	R	1.29	5	I	1.30	5
SA 38 SF1	2	B	1.17	130	V	1.18	60	R	1.19	60	I	1.19	60
SA 38 SF4	13	B	1.19	160	V	1.21	20	R	1.22	10	I	1.22	10
SA 41 SF1	13	B	1.01	230	V	1.02	200	R	1.02	200	I	1.02	200
SA 41 SF2	5	B	1.03	150	V	1.04	20	R	1.04	20	I	1.04	20

zero point) and slope (extinction coefficient):

$$B = b_0 + \zeta_b = b_i - k_b X + \zeta_b, \quad (10)$$

$$V = v_0 + \zeta_v = v_i - k_v X + \zeta_v, \quad (11)$$

$$R = r_0 + \zeta_r = r_i - k_r X + \zeta_r, \quad (12)$$

$$I = i_0 + \zeta_i = i_i - k_i X + \zeta_i, \quad (13)$$

where *BVRI* are the standard stars' magnitudes taken from the catalog,  $\zeta_{b,v,r,i}$  are the magnitude zero point offsets between the instrumental and the standard system, and  $k_{b,v,r,i}$  are the extinction coefficients in each *BVRI* filter used.

#### 4.2. Calibration with color correction

Color shifts between ours (*BVRI*) and standard stars' filters (*BVRI*) can be quantified by the following set of equations:

$$B = b_i - k_b X + \epsilon_b(B - V) + \zeta_b, \quad (14)$$

$$V = v_i - k_v X + \epsilon_v(B - V) + \zeta_v, \quad (15)$$

$$R = r_i - k_r X + \epsilon_r(V - R) + \zeta_r, \quad (16)$$

$$I = i_i - k_i X + \epsilon_i(V - I) + \zeta_i, \quad (17)$$

where  $\epsilon_{b,v,r,i}$  are color terms for particular colors. More equations of this kind can be written to address all possible combinations of filters used. The air mass *X* is the average value of air masses corres-

ponding to the air masses of observations taken with two different filters since the fields cannot be imaged simultaneously.

In the case of additional correction for extinction in the  $B$ -band, the extinction coefficient  $k_b$  in the above equation should be replaced with the expression given by Eq. (5). Since this effect is very small, this correction should be applied only in the case of well sampled data regarding the color range.

## 5. RESULTS

All the equations derived here for different corrections, can be solved by multiple regression. However, since we have errors both in dependent and independent variables, we have chosen to apply the orthogonal distance regression that takes into account measurement errors in all variables.

We have used ODRPACK (ODR) package from SciPy v1.6.1 library in Python (Virtanen et al. 2020). ODRPACK is actually a FORTRAN-77 library for performing orthogonal distance regression with possibly non-linear fitting functions (Boggs et al. 1989). It is based on a Levenberg-Marquardt-type algorithm including weights to account for different variances of the observations.

Photometric calibration with and without the color term was done by creating a model and applying an orthogonal distance regression to it. The code is available at Github.<sup>4</sup> In the simple case of correcting only for the extinction (Subsection 4.1), the calibrated magnitude in the  $B$ -band, along with residuals  $\Delta B = B_{\text{cal}} - B$  (where  $B_{\text{cal}}$  stands for the calibrated magnitude and  $B$  refers to the standard stars magnitude) is given in Fig. 1. In a more complex case with the color correction (Subsection 4.2), the calibrated magnitude with distribution of residuals is given in Fig. 2. Residuals are always the difference between the calibrated magnitude and the standards' stars one; only the calibrated magnitude will consist simply of the magnitude zero point and the extinction coefficient in the simple case of extinction correction, while it will additionally have the color term correcting for the color dependence in a more complicated case with color correction that we apply and discuss its importance.

In the  $B$ -band, it can easily be seen by comparing residuals in Fig. 1 and Fig. 2 that the error of the calibrated magnitude is smaller and that the distribution of residuals is closer to a normal distribution by taking the color correction into account. The errors consist of measurement errors and statistical errors from the fitted parameters added in the quadrature. So, the reason why the errors in the latter case are smaller simply refers to the smaller errors of the fitted parameters (the magnitude zero point and extinction coefficient).

To test the significance of the level at which the two residual distributions (with and without the color correction) are close to the normal one, we have performed three statistical test: Shapiro-Wilk (Shapiro and Wilk (1965); `shapiro` SciPy function), Anderson-Darling (Anderson and Darling (1954); `anderson` SciPy function) and D'Agostino's  $K^2$  test (D'Agostino (1970); `normaltest` SciPy function). These are the most commonly used statistical tests, each of them taking different assumptions and considering a different aspect of data. They all test the null hypothesis – normality of the residual distribution. Each test delivers both a statistics and  $p$ -value; statistics is compared to some pre-calculated critical value for a particular test, and the  $p$ -value is a measure of probability that the difference between the distribution of residuals and normal distribution (in our case) may occur by a random chance: higher the  $p$ -value, stronger is the evidence in favor of the null hypothesis and vice versa. The SciPy implementation of these tests, yields the following interpretation: if  $p > \alpha$ , than our assumption holds. The significance value  $\alpha$ , which we use for comparison with the measured  $p$ -value, is some (predefined) probability of rejecting the null hypothesis that is actually true, i.e. it is a probability of making a wrong decision. This parameter is by convention set to  $\alpha = 0.05$ , meaning that there is a probability of 5% that we claim the residual distribution is normal, while it is not.

To summarize, we will measure the  $p$ -values for each of statistical tests and compare them with the  $\alpha$  value. If the  $p$ -value is larger than  $\alpha$ , than our null hypothesis (assumption that residuals follow the normal distribution) holds. Why is this important? Residuals should be randomly distributed, or else either the model is not correct (calibration equations), or our data sample is small, or simply data are not well distributed over the range of our dependent variable(s). The consequence is that our model cannot successfully predict (calibrate) magnitudes for the given particular data set. Normality assumption, along with calculated errors, can also help us choose the most appropriate model for our data. On the other hand, errors of the fitted parameters should also be considered, since in the case they are comparable to the parameters themselves, models that introduce them should be disfavored with respect to simpler ones. We need to take all this into account when choosing the model that is the most appropriate for the given data set.

We run all three tests, since they inspect different features of the residual distribution they are fed with. The Anderson-Darling test, for example, pays more attention to the wings of the distribution, and these are the areas where we visually see the difference from the normal distribution (in all figures with residuals in all bands, the left wing is somewhat skewed). We shall demand that all the tests agree with the normality assumption for the distribution of residuals.

<sup>4</sup>[https://github.com/anavudragovic/photometry/blob/master/stdphot\\_secext.py](https://github.com/anavudragovic/photometry/blob/master/stdphot_secext.py)

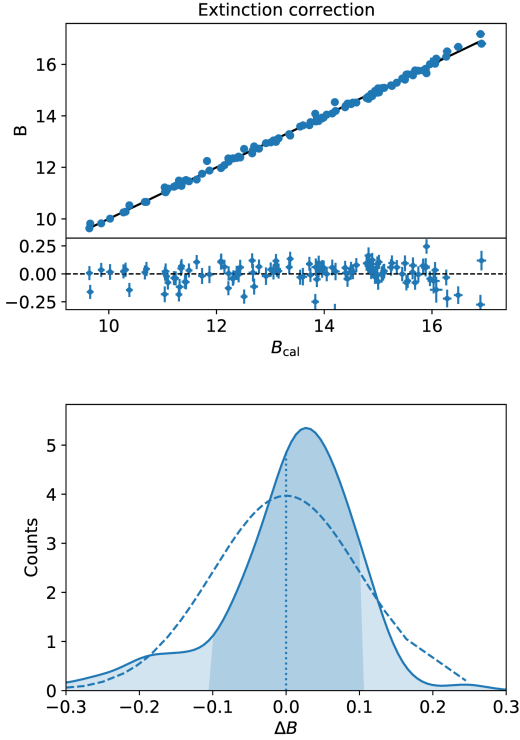


**Fig. 1:** Photometric calibration with extinction correction only: (above) calibrated  $B$ -band magnitude with residuals shown in the lower part of the plot, (below) residuals with shaded area corresponding to the standard deviation  $\sigma = 0.1$ ; dashed line is the normal distribution overplotted.

All the tests reject the normality assumption for the simple extinction correction in the  $B$ -band (Fig. 1), and fail to reject the same assumption with color correction applied (Fig. 2) at the significance level of  $\alpha=0.05$ . For the  $V$ -band, there is no difference between the tests performed on residuals in both cases (with and without color correction). The distribution of residuals is not normal for either the  $R$ - or  $I$ -band: with or without the color correction, so there is no need to apply the additional correction too (Fig. 5 - 8). In addition, the standard deviation of residuals is the same at 0.01 magnitude level (1% accuracy) for the  $V$ -,  $R$ - and  $I$ -band.

We have also tested an additional correction, the second order extinction correction in the  $B$ -band (Eq. 5). Although the residuals behave well and the normality assumption is satisfied, the errors of the fitted parameters grew large, in some cases they are even larger than the parameters themselves, implying that this additional effect cannot be measured from these data. Maybe, if the data spanned a larger range in colors, an additional correction could be applied.

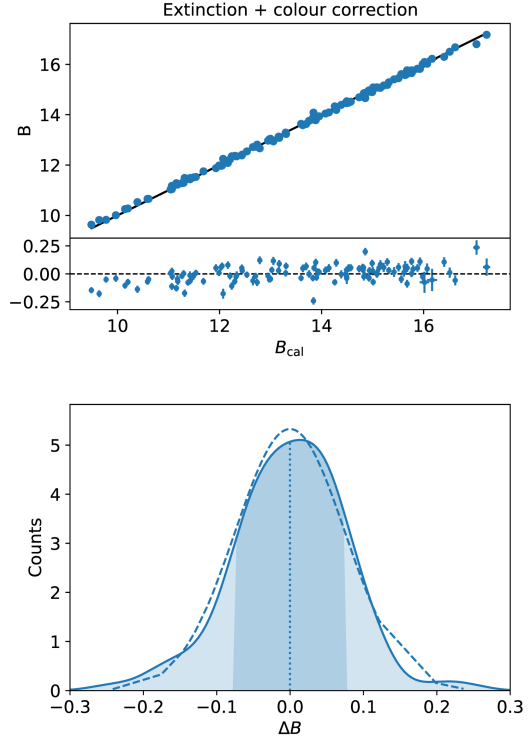


**Fig. 2:** Photometric calibration with extinction and color correction: (above) calibrated  $B$ -band magnitude with residuals shown in the lower part of the plot, (below) residuals with shaded area corresponding to the standard deviation  $\sigma = 0.08$ ; dashed line is the normal distribution overplotted.

**Table 3:** Results of the photometric calibration:  $\zeta$  is the magnitude zero point for a given filter  $f = BVRI$  (the first column),  $k$  is the extinction coefficient (the second column) and  $\epsilon$  is the color term (the last column). Those rows that are printed in bold are the most appropriate for given filters.

$\zeta_f$ [mag]	$k_f$ [mag/air mass]	$\epsilon_f$
$B$		
$21.78 \pm 0.05$	$0.48 \pm 0.04$	/
<b><math>21.32 \pm 0.02</math></b>	<b><math>0.19 \pm 0.01</math></b>	<b><math>0.17 \pm 0.02</math></b>
$V$		
<b><math>22.11 \pm 0.03</math></b>	<b><math>0.37 \pm 0.03</math></b>	/
$22.08 \pm 0.03$	$0.36 \pm 0.03$	$0.02 \pm 0.01$
$R$		
<b><math>22.12 \pm 0.05</math></b>	<b><math>0.48 \pm 0.04</math></b>	/
$22.15 \pm 0.05$	$0.51 \pm 0.04$	$0.01 \pm 0.04$
$I$		
<b><math>21.26 \pm 0.02</math></b>	<b><math>0.16 \pm 0.01</math></b>	/
$21.20 \pm 0.02$	$0.15 \pm 0.01$	$0.06 \pm 0.02$

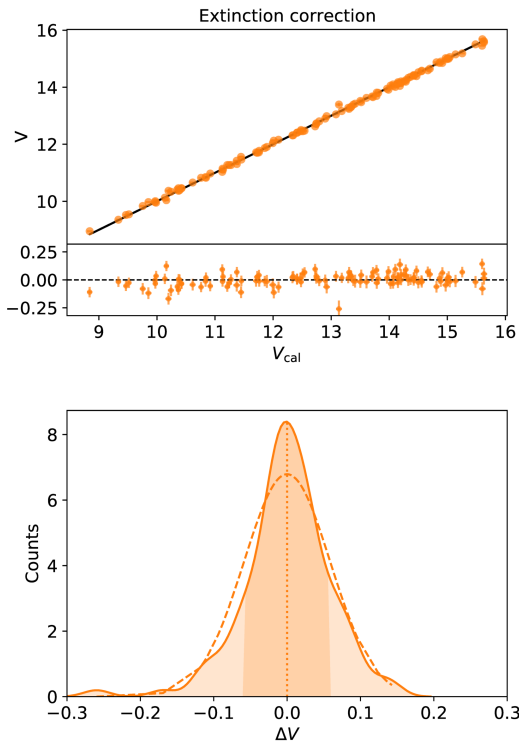


**Fig. 3:** Same as in Fig. 1 for  $V$ -band and  $\sigma = 0.06$ .

We conclude that the color correction is relevant only for the  $B$ -band. In the  $V$ -,  $R$ - and  $I$ -band, a simple extinction correction suffices. The magnitude zero points, extinction coefficients, and a single color term (in the  $B$ -band) with their corresponding errors are given in Table 3. For the purpose of comparison, we give the measured parameters for both cases, with and without the color correction, but those that are correct considering both residual distribution and errors of the measured parameters are printed in bold. For example, in the  $B$ -band, all errors of the fitted parameters get smaller when the color correction is applied (the first two rows in Table 3). It can also be seen visually in the bottom of the upper panel in Fig. 2 if compared to Fig. 1. Moreover, the lower panels of the same two figures representing the distribution of residuals of the calibrated vs. true (standard stars) magnitude, reveal a different behaviour of the two models (without and with the color correction) with respect to the normal distribution (dashed line), which is seen in different  $p$ -values: 0.00 vs. 0.01 for the Shapiro-Wilk test or 0.00 vs. 0.093 for D’Agostino’s  $K^2$  test. These  $p$ -values should be larger than  $\alpha=0.05$  and this is true in the case when the color correction is applied for both tests. For the Anderson-Darling test, the critical value of the test at the 5% significance level (0.76) is compared to the measured one in both cases (without and with the color correction):  $3.355 > 0.76$  vs.  $0.537 < 0.76$ ; in the first case, the measured value, being

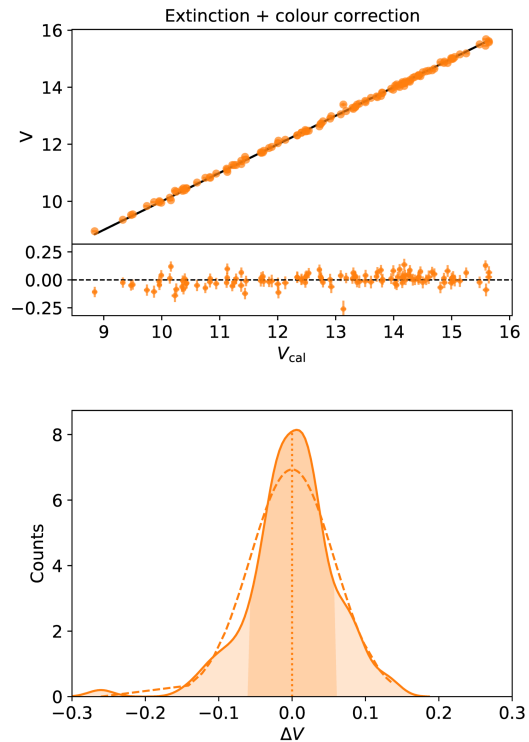


**Fig. 4:** Same as in Fig. 2 for  $V$ -band and  $\sigma = 0.06$ .

larger than the critical one, implies that the distribution of residuals is not normal, while in the latter case it implies the opposite. All the tests agree upon the normality assumption in the latter case and this model, the one with the color correction, is favored over the more simpler one and is printed in bold in Table 3. In all other bands ( $V$ ,  $R$ ,  $I$ ) the statistics doesn’t play a big role. Both residual distributions (without and with color correction) are not normal according to all statistical tests. There is an additional argument why the simpler model is more appropriate for these bands. In Table 3, for all except for the  $B$ -band, the additional color term (normal font line, not bold) has the error that is comparable or even larger than the value of the parameter, meaning that it cannot be determined from these data. So, for all other bands, we favour the simple extinction correction (bold in Table 3).

We suspect the reason for unsuccessful determination of color terms is related to the modest range in colors  $B - V = (0.0, 1.3)$ . We lack both genuinely blue ( $B - V < 0$ ) and red stars ( $B - V > 1.4$ ) in our data set. On the other hand, this color range corresponds to the color of RU Camelopardalis (RU Cam) star that was the primary motivation for accurate photometric calibration, so our results can be applied to this star.

RU Cam is a long period pulsating star, a  $V$  Virginis subtype of Type II Cepheid. In the past it showed changes in the amplitude of the pulsation and

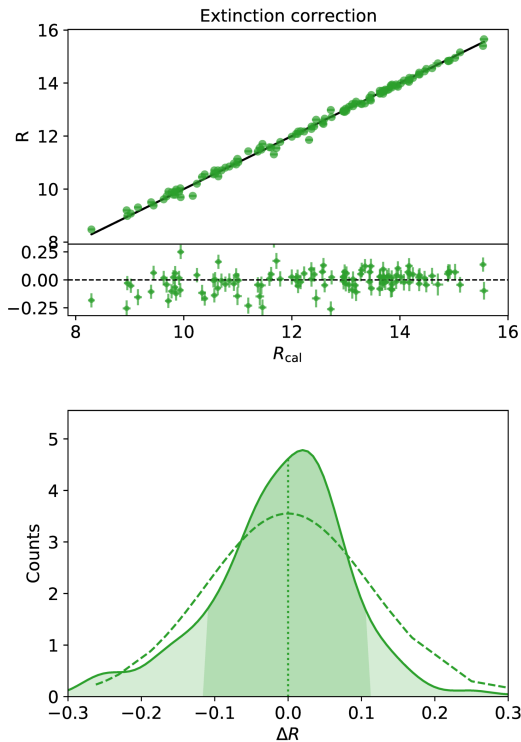


Fig. 5: Same as in Fig. 1 for  $R$ -band and  $\sigma = 0.1$ .

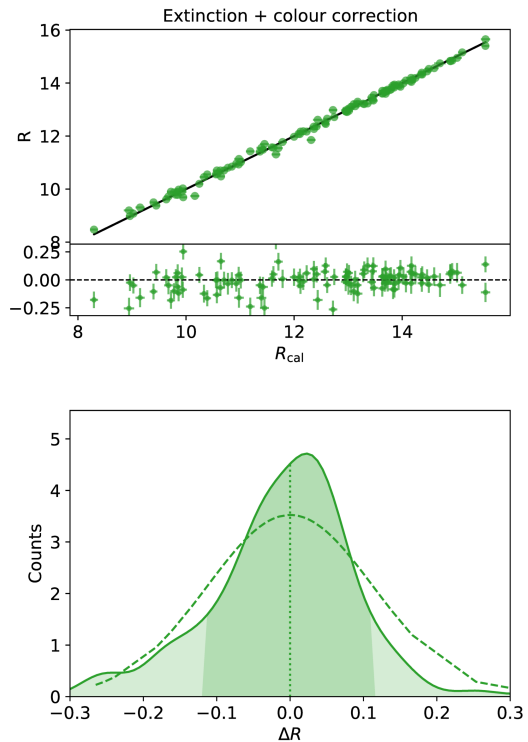


Fig. 6: Same as in Fig. 2 for  $R$ -band and  $\sigma = 0.1$ .

length of pulsation cycle on a time scale of decades. We are observing the light curve in different filters to determine the nature of these changes. RU Cam is just one of the Type II Cepheids and anomalous Cepheids that are going to be observed at the ASV. Some Type II Cepheids show small changes in their amplitude that repeat every second period, so the phenomenon is called the period doubling (PD). The detection requires a precision of the order of few hundredths of magnitude. To study these changes it is required that we observe these stars for a very long time – decades or longer. Such long observations entail that the telescopes, as well as the observing equipment, will change, and the easiest way to overcome the different compensation among different systems is to anchor each and every observation to a standard photometric system. The big automated observing programs (for example Optical Gravitational Lensing Experiment<sup>5</sup> use either the  $BVRI$  filters or the  $ugriz$  filters. The standard photometry also becomes important when one takes into account that these pulsating stars change their effective temperature during the pulsation cycle. This would mean that finding an appropriate comparison star (if there is one in the same observing field) would only approximate the spectral type of the pulsating star. Using the standard photometric calibration we deal with the color correction, increase the precision of our photometry,

<sup>5</sup><http://ogle.astrouw.edu.pl/>

Table 4: Measured sky brightness in the magnitudes per arcsec squared in the  $BVRI$  bands for three observing nights, from 5th August to 7th August.

f	5th August	6th August	7th August
$B$	$21.29 \pm 0.03$	$21.22 \pm 0.08$	$19.85 \pm 0.10$
$V$	$20.86 \pm 0.13$	$20.43 \pm 0.15$	$19.39 \pm 0.20$
$R$	$20.17 \pm 0.06$	$20.05 \pm 0.10$	$19.18 \pm 0.08$
$I$	$18.77 \pm 0.04$	$19.28 \pm 0.21$	$18.42 \pm 0.06$

make it accessible for other long term programs to incorporate, and at the end it is also a long-standing consensus of the variable star community.

## 6. PHOTOMETRIC CONDITIONS

Photometric calibration due to high precision demands clear, dark skies. There are no previous measurements of the sky darkness at the ASV. We have measured the surface brightness of the sky during observations as the mean flux of median values inside dozen boxes of 50 times 50 pixels size in the areas without objects. These values are then converted into the surface brightness by dividing the flux with the area of one pixel in arcseconds and then calibrated using photometric calibration coefficients from the Table 3.

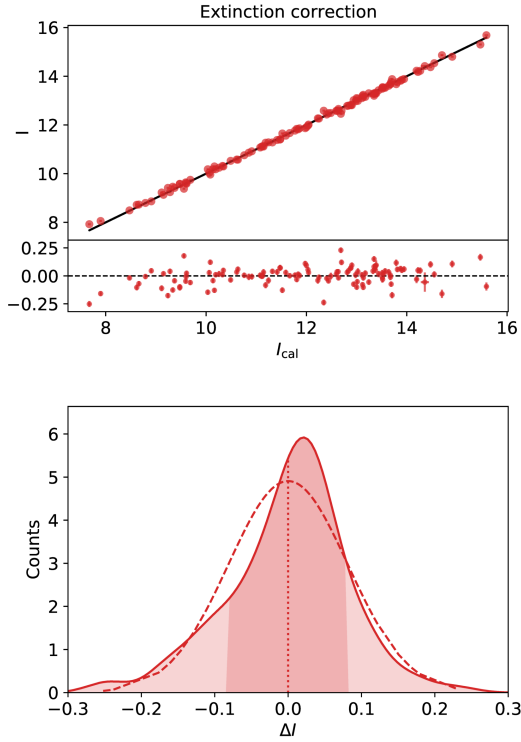


Fig. 7: Same as in Fig. 1 for  $I$ -band and  $\sigma = 0.08$ .

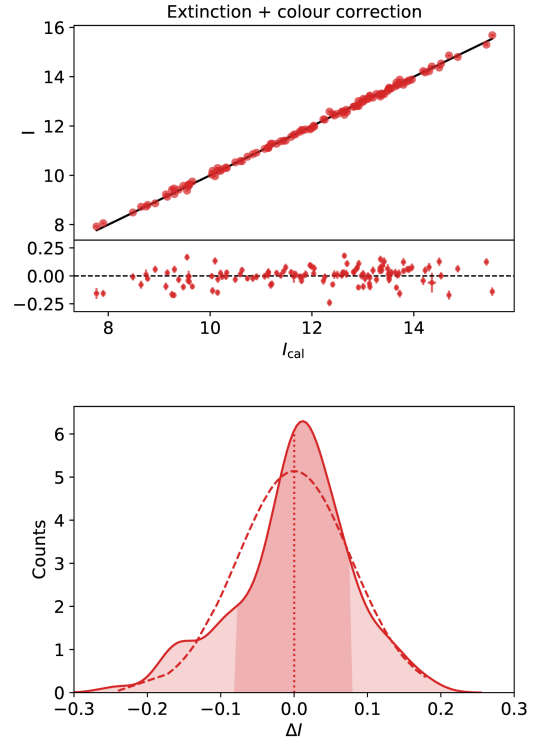


Fig. 8: Same as in Fig. 2 for  $I$ -band and  $\sigma = 0.08$ .

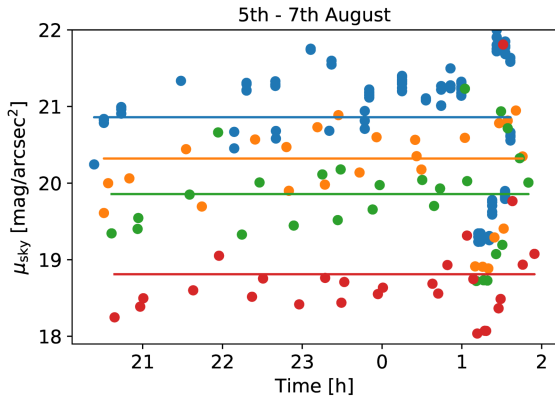


Fig. 9: Sky surface brightness in magnitudes per arcsec squared during the observing nights from 5th to 7th August, color coded according to the filter used: blue ( $B$ ), orange ( $V$ ), green ( $R$ ), and red ( $I$ ). Horizontal lines – colored according to the filter used – mark the mean value of sky brightness.

Measurements of the sky brightness are listed in the Table. 4 for each night. Photometric calibration was done by using measurements from all three nights together (Fig. 9) and, in this case, when all the nights are taken together, the measured sky brightness is:  $20.86 \pm 0.07$ ,  $20.32 \pm 0.09$ ,  $19.86 \pm 0.06$ ,

$18.81 \pm 0.07$  in the  $BVRI$  bands, respectively (horizontal lines at Fig. 9). Standard error of the mean sky brightness is similar to variations in calibrated magnitudes expressed as the standard deviation of residuals between calibrated and standard magnitudes: 0.08, 0.06, 0.11 and 0.08 in the  $BVRI$  bands (shaded area in Figs. 2 - 8).

The Moon was transiting from the New Moon phase (which was on the 1st August, 2019) to the First Quarter, which was exactly on the 7th August, 2019. Observing at this time minimized the effect of the moonlight on sky brightness.

The time lapse videos from the All Sky camera installed at the ASV shows that the nights of the 5th, 6th and 7th August, 2019 were clear nights, without clouds<sup>6</sup>, making them ideal for photometric calibration observations.

## 7. CONCLUSION

We have observed 31 field of standard stars in the  $BVRI$  Johnson's photometric system, selected from Landolt's catalog of standard stars with the 60 cm Nedeljković telescope equipped with a FLI PL 230 CCD camera. Observations are conducted during three nights in August, 2019 at zenith distances

<sup>6</sup><https://www.youtube.com/watch?v=CrQTzXtBpcs>, <https://www.youtube.com/watch?v=R3aZPefB2MA> and <https://www.youtube.com/watch?v=BJUqi5-4XhY>

$z < 60^\circ$ . We have done photometric calibration both with and without the color term in the  $B$ -,  $V$ -,  $R$ - and  $I$ -bands. Calibration coefficients, measured by means of orthogonal distance regression, are then used to transform the instrumental to calibrated magnitudes. A simple extinction correction is sufficient in all bands, except for the  $B$ -band, where the additional color correction need to be applied. The accuracy achieved by inspecting magnitude errors that encompass both measurement and statistical errors added in the quadrature, is between 2% and 5% for all  $BVRI$  bands.

*Acknowledgements* – We acknowledge the financial support of the Ministry of Education, Science and Technological Development of the Republic of Serbia through the contract No. 451-03-9/2021-14/200002. We thank the Director of the Astronomical Observatory of Belgrade, Dr Gojko Đurašević, for giving us his observational time for this project, and the technical operators at the ASV, Miodrag Sekulić and Petar Kostić for their excellent work. This research made use of Photutils, an Astropy package for detection and photometry of astronomical sources.

## REFERENCES

- Anderson, T. W. and Darling, D. A. 1954, Journal of the American Statistical Association, 49, 765
- Boggs, P. T., Donaldson, J. R., Byrd, R. h. and Schnabel, R. B. 1989, ACM Trans. Math. Softw., 15, 348
- Bradley, L., Sipőcz, B., Robitaille, T., et al. 2020, [astropy/photutils: 1.0.0](#)
- D’Agostino, R. B. 1970, Biometrika, 57, 679
- Henden, A. A. and Kaitchuck, R. H. 1982, Astronomical photometry (New York: Van Nostrand Reinhold)
- Landolt, A. U. 2013, [AJ](#), 146, 131
- Lang, D., Hogg, D. W., Mierle, K., Blanton, M. and Roweis, S. 2010, [AJ](#), 139, 1782
- Müller, O., Vudragović, A. and Bílek, M. 2019, [A&A](#), 632, L13
- Shapiro, S. S. and Wilk, M. B. 1965, Biometrika, 52, 591
- Vince, O., Cvetković, Z., Pavlović, R., Damjanović, G. and Djurašević, G. 2014, [Contributions of the Astronomical Observatory Skalnaté Pleso](#), 43, 368
- Vince, O. and Jurkovic, M. 2012, [POBeo](#), 91, 77
- Virtanen, P., Gommers, R., Oliphant, T. E., et al. 2020, [Nature Methods](#), 17, 261
- Young, A. T. and Irvine, W. M. 1967, [AJ](#), 72, 945

***BVRI* ФТОМЕТРИЈСКА КАЛИБРАЦИЈА ТЕЛЕСКОПА НЕДЕЉКОВИЋ****A. Vudragović and M. I. Jurkovic***Astronomical Observatory, Volgina 7, 11060 Belgrade, Serbia*E-mail: [ana@aob.rs](mailto:ana@aob.rs)

УДК 520.8.07 + 520.823

*Стручни чланак*

У овом чланку смо описали фотометријску калибрацију 60 см телескопа Недељковић са FLI PL 230 CCD камером, који је постављен на Астрономској станици Видојевица (Србија), помоћу Ландолтовог каталога стандардних звезда. Направили смо снимке 31. поља стандардних звезда користећи Цон-

сонове  $BVRI$  филтере, током три ноћи у августу 2019. године. Израчунали смо корекцију на екстинкцију и боју. Поредили калибрисане магнитуде са магнитудама стандардних звезда из Ландолтовог каталога, постигли смо тачност од 2%-5% за  $BVRI$  магнитуде.